Applied Physics Letters

RESEARCH ARTICLE | OCTOBER 17 2024

Optimization of the dielectric layer parameters through coupled numerical analysis to enhance droplet and particle manipulation in digital microfluidic chips

Yanfeng Zhao ; Menghua Liu ; Xinyi Dong ; Jiaxin Liu ; Hen-Wei Huang ; Qing Shi ; Qiang Huang ; Huaping Wang

Appl. Phys. Lett. 125, 163702 (2024)
https://doi.org/10.1063/5.0225853

13 November 2024 03:12:15

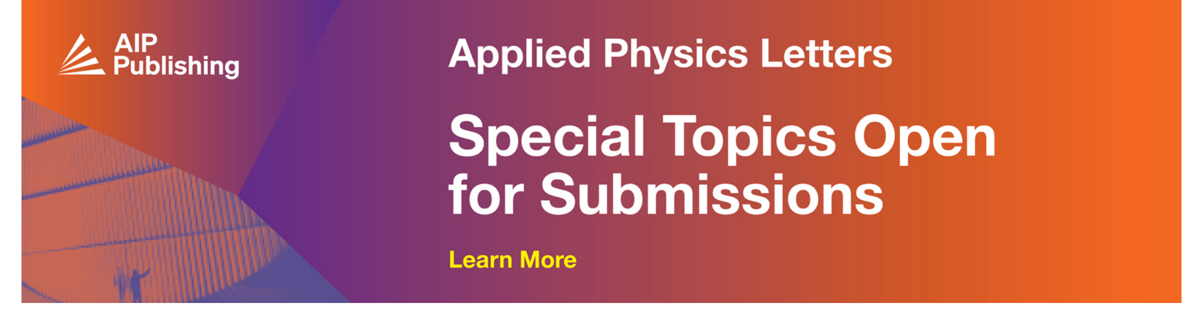

Applied Physics Letters ARTICLE pubs.aip.org/aip/apl

Optimization of the dielectric layer parameters through coupled numerical analysis to enhance droplet and particle manipulation in digital microfluidic chips

Cite as: Appl. Phys. Lett. **125**, 163702 (2024); doi: 10.1063/5.0225853
Submitted: 27 June 2024 · Accepted: 9 October 2024 ·
Published Online: 17 October 2024

View Online

Export Citation
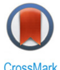
CrossMark

Yanfeng Zhao,[1] Menghua Liu,[1] Xinyi Dong,[1] Jiaxin Liu,[1] Hen-Wei Huang,[2] Qing Shi,[3] Qiang Huang,[3] and Huaping Wang[4,a)]

AFFILIATIONS

[1]Intelligent Robotics Institute, School of Mechatronical Engineering, Beijing Institute of Technology, Beijing 100081, China
[2]Nanyang Assistant Professor at School of Electrical and Electronic Engineering and the LKC School of Medicine, Nanyang Technological University, Singapore
[3]Beijing Advanced Innovation Center for Intelligent Robots and Systems, Beijing Institute of Technology, Beijing 100081, China
[4]Key Laboratory of Biomimetic Robots and Systems (Beijing Insitite of Technology), Ministry of Education, Beijing 100081, China

[a)]**Author to whom correspondence should be addressed:** wanghuaping@bit.edu.cn

13 November 2024 03:12:15

ABSTRACT

Digital microfluidic chips (DMCs) have shown the ability to flexibly manipulate droplets and particles, which is meaningful for biomedical applications in drug screening and clinical diagnostics. As a critical component of DMCs, the dielectric layer, with its key physical parameters (permittivity and thickness), directly determines the voltage distribution, thereby significantly affecting the manipulation performance. To optimize manipulation performance, simulation studies on dielectric layer parameters are essential during the DMC design. Existing simulation methods can evaluate the effect of dielectric layer parameters on droplet manipulation but encounter inherent challenges when analyzing the manipulation of particles within droplets. Here, we propose a versatile numerical analysis approach that can simultaneously analyze the effect of dielectric layer parameters on both droplet and particle manipulation, thereby optimizing the dielectric layer parameters to enhance the DMC manipulation performance. Initially, the voltage distributions corresponding to different sets of dielectric layer parameters are solved using electromagnetic field theory. Subsequently, the voltage distribution data are used to calculate the droplet and particle driving forces based on the principle of virtual work. Finally, by comparing the driving forces across different sets of dielectric layer parameters, the optimal dielectric layer parameters are determined to enhance the DMC manipulation performance. Experimental results demonstrate that the droplet and particle accelerations align with the simulated driving force trends, thereby validating our numerical analysis method. We anticipate that our method will be able to provide theoretical guidance for the optimization of dielectric layer parameters to obtain a desirable manipulation performance in more complex DMC designs.

Published under an exclusive license by AIP Publishing. https://doi.org/10.1063/5.0225853

Digital microfluidic devices, which are emerging as versatile platforms for microfluidic manipulation, are being increasingly applied in critical areas such as medical diagnostics,[1–3] biochemical research,[4,5] and cellular studies.[6,7] With the continuous advancement of digital microfluidics, the manipulation of particles within droplets is becoming indispensable for a growing range of applications.[8–10] The droplet and particle manipulation in a digital microfluidic chip (DMC) is controlled by working electrodes that generate an essential driving force.[11,12] These electrodes are coated with a dielectric layer, which is a critical component that directly impacts the manipulation performance.[13] Inappropriate selection of dielectric layer parameters, such as the permittivity and thickness, can result in operation failure or even dielectric breakdown, potentially damaging the DMC. Current methods for analyzing the effect of the dielectric layer parameters on droplet manipulation performance typically employ direct current excitation.[14,15] However, this approach limits the analysis of particle manipulation and overlooks frequency effects on the droplet performance. Overcoming these limitations to simultaneously analyze the effects of

the dielectric layer parameters on both droplet and particle manipulation remains a critical challenge.

In this study, we introduce a versatile numerical analysis approach for evaluating how the permittivity and thickness of the dielectric layer affect the droplet and particle manipulation performance in a DMC. We constructed a finite element model of the DMC and used electromagnetic field theory for simulation to obtain the voltage distribution data. By varying the dielectric layer parameters, a series of voltage distribution data was generated. By utilizing these data, we calculated the driving force acting on both the droplets and particles. By comparing the driving forces, we identified the dielectric layer parameter values corresponding to the maximum driving force, which represent the optimal parameter values. We used DMCs to conduct driving experiments of droplets and particles, in which their accelerations were calculated. The experimental results show that the accelerations of droplets and particles match the simulation results, confirming the validity of our numerical analysis approach. In summary, our innovative numerical analysis approach enables comprehensive analysis of the effect of dielectric layer parameters on the DMC manipulation performance, which offers great potential for the optimal design of DMCs.

The composition of the DMC used in this study is illustrated in Fig. 1(a). The chip consists of two vertically stacked substrates. The top substrate is a glass panel coated with an indium tin oxide (ITO) layer and a hydrophobic layer.[16] Similarly, the bottom substrate, also constructed from glass, is coated with an ITO layer, a dielectric layer, and a hydrophobic layer. The influence of the hydrophobic layer is disregarded due to its minimal thickness. For the voltage distribution within the DMC, the dielectric layer and the droplet are primarily focused on, as shown in Fig. 1(b). V_1 is designated as the voltage of the droplet, and V_2 represents the voltage across the dielectric layer. As shown in Fig. 1(b), droplet manipulation within the DMC is achieved through the electrowetting-on-dielectric (EWOD) force, whereas particle manipulation within the droplets is accomplished using the dielectrophoresis (DEP) force. Therefore, we propose a versatile numerical analysis method, combined with simulation to obtain the voltage distribution and an empirical formula to calculate the force. This method allows us to calculate the EWOD force and DEP force under the same excitation conditions, as shown in Fig. 1(c).

To quantitatively assess the effect of dielectric layer parameters on the DMC manipulation performance, we solved the voltage distribution for EWOD and DEP based on electromagnetic field theory simulation. The relevant dimensions used in the simulation are detailed in the supplementary material (Table I). Our initial simulation analysis focused on EWOD, with the modeling settings depicted in the supplementary material (Fig. S1). The EWOD force, which is responsible for propelling droplets within a DMC, can be derived from the Laplace–Young and Young–Lippmann equations:[17]

$$F_{EWOD} = \frac{\varepsilon_0 \varepsilon_D L}{2d} V_2^2, \quad (1)$$

where ε_0 is the permittivity of vacuum, ε_D is the dielectric layer permittivity, d is the dielectric layer thickness, and L is the electrode width.

As demonstrated in Eq. (1), the EWOD force is influenced by several factors, including the permittivity and thickness of the dielectric layer as well as the voltage across the dielectric layer (V_2). Notably, V_2 is determined by the combination of dielectric layer parameters, along with the amplitude and frequency of the applied voltage. We conducted extensive simulations to obtain V_2. These simulations enabled us to evaluate the effects of the amplitude and frequency of the applied

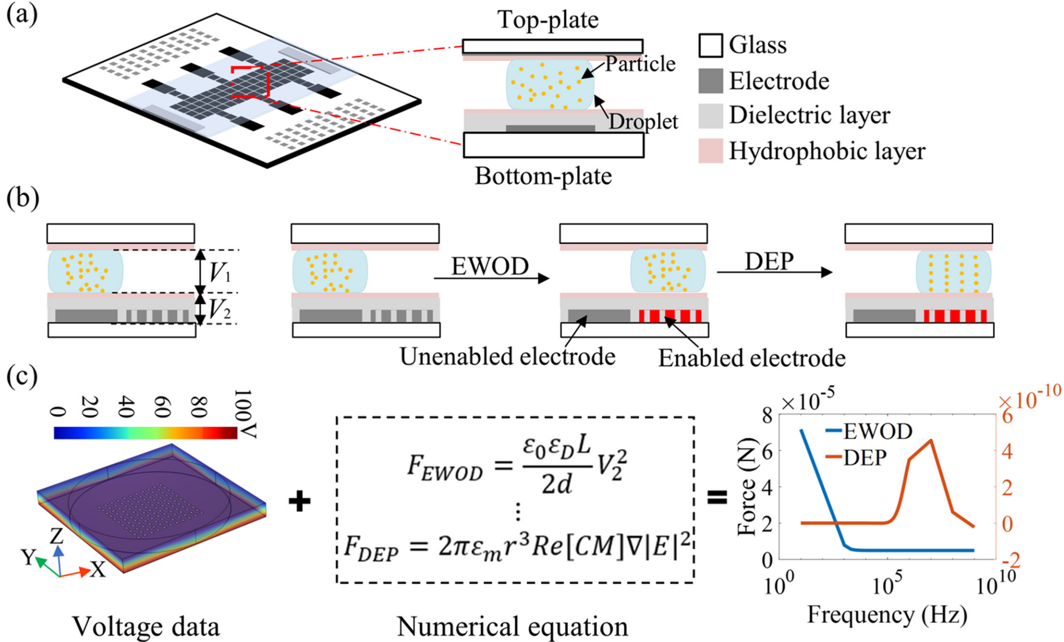

FIG. 1. Diagrams of the composition of, operation of, and numerical analysis method for a DMC. (a) Schematic diagram of the components of a DMC. (b) Schematic diagram of the basic manipulation of a DMC. (c) Schematic diagram of the method for numerically analyzing a DMC.

13 November 2024 03:12:15

Published under an exclusive license by AIP Publishing

voltage and dielectric layer parameters on V_2. Using the simulated V_2 values, we calculated the EWOD force, which allowed a comprehensive analysis of how changes in the permittivity and thickness of the dielectric layer affect the driving force generated by EWOD.

The cross-sectional view in Fig. 2(a) illustrates the simulated voltage distribution within the DMC. In Fig. 2(b), the graph depicts the correlation between V_2 and the amplitude and frequency of the applied voltage. V_2 consistently increases with increasing amplitude at a constant frequency and decreases with increasing frequency at a constant amplitude. To further investigate the impact of permittivity on V_2, we selected six dielectric materials: PDMS (2.71), Parylene C (3.15), SU-8 (3.6), SiO_2 (4.5), Al_2O_3 (8.8), and Ta_2O_5 (23) with gradually increasing permittivities. The variation trend of V_2 under different dielectric layer permittivities is shown in Fig. 2(c). These results indicate that at a constant frequency, V_2 decreases with increasing permittivity. At various permittivities, V_2 exhibits consistent trends with changing frequency. In Fig. 2(d), the variation trend of V_2 under different dielectric layer thicknesses is shown. These results indicate that a higher permittivity results in a lower V_2 for a given thickness. For the same permittivity, a thicker dielectric layer results in a higher V_2. The variations in the EWOD force under different permittivities and thicknesses of the dielectric layer are shown in Figs. 2(e) and 2(f). As shown in Fig. 2(e), the EWOD force decreases with decreasing permittivity [Fig. S2(a)] but maintains a notable force level ($10^{-4} \sim 10^{-5}$ N) in the frequency range $<10^3$ Hz because within this frequency range, there is minimal variation in V_2 for dielectric layers with different permittivities, as shown in Fig. 2(c). Therefore, the EWOD force has a positive correlation with the permittivity. In contrast, in the frequency range $\geq 10^3$ Hz, the EWOD force increases with decreasing permittivity [Fig. S2(b)] but remains relatively small. This occurs because, in this frequency range, significant variations in V_2 are observed for dielectric layers with different permittivities, and the V_2 values are smaller for the dielectric layers with higher permittivities, as shown in Fig. 2(c). Therefore, the EWOD force is negatively correlated with the permittivity. As shown in Fig. 2(f), at 10^3 Hz, the EWOD force gradually increases with increasing dielectric layer thickness for Ta_2O_5. However, for other materials, the EWOD force initially increases and subsequently decreases with increasing thickness. This finding contrasts with the trend at 10^2 Hz, as shown in the supplementary material (Fig. S3). This suggests that an optimal thickness exists for each material to maximize the EWOD force at a given frequency. Based on the aforementioned analysis, the optimal applied frequency for enhanced performance should be in the low-frequency range. Selecting a dielectric material with a higher permittivity is advisable. The optimal thickness for maximizing the EWOD force should be ascertained through simulation calculations.

The DEP force acting on particles in a droplet can be formulated as follows:[18]

$$F_{DEP} = 2\pi\varepsilon_m r^3 \mathrm{Re}[CM]\nabla|E|^2, \tag{2}$$

$$\mathrm{Re}[CM] = \mathrm{Re}\left[\frac{\varepsilon_p^* - \varepsilon_m^*}{\varepsilon_p^* + 2\varepsilon_m^*}\right], \tag{3}$$

where ε_m is the permittivity of the solution, r is the radius of the particles, $\mathrm{Re}[CM]$ is the real part of the Clausius–Mossotti (CM) factor, and $\nabla|E|^2$ is the gradient of the square of the electric field strength. $\varepsilon^* = \varepsilon - j\sigma/\omega$, where ε and σ are the permittivity and conductivity, respectively. The subscripts p and m denote the particle and the solution, respectively. In addition, $\omega = 2\pi f$, where f is the frequency of applied voltage.

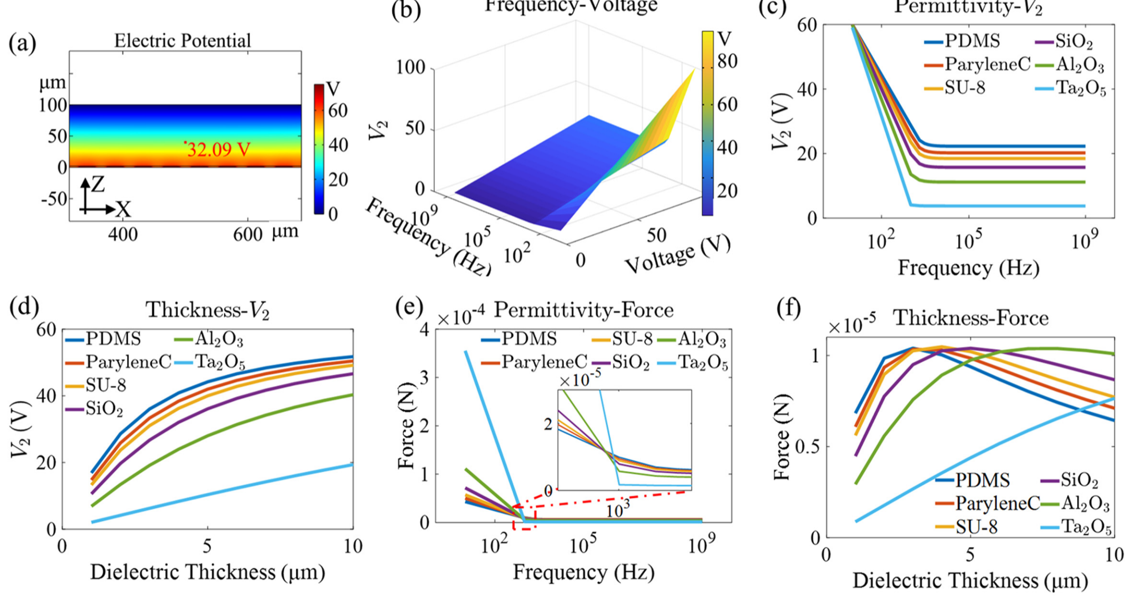

FIG. 2. EWOD simulation results. (a) Cross section of the simulated voltage distribution ($\varepsilon_D = 3.6$, d = 2 μm, applied voltage = 100 V, frequency = 10^3 Hz). (b) Correlation of V_2 with the amplitude and frequency of the applied voltage ($\varepsilon_D = 3.6$, d = 2 μm). (c) Correlation between V_2 and the dielectric layer permittivity ($\varepsilon_D = 3.6$, d = 2 μm). (d) Correlation between V_2 and the dielectric layer thickness (frequency = 10^3 Hz). (e) Correlation between the EWOD force and the dielectric layer permittivity ($\varepsilon_D = 3.6$, d = 2 μm). (f) Correlation between the EWOD force and the dielectric layer thickness ($\varepsilon_D = 3.6$, d = 2 μm).

13 November 2024 03:12:15

Published under an exclusive license by AIP Publishing

As demonstrated in Eq. (2), when the properties of the solution and particles are fixed, key parameters such as the permittivity and conductivity of both remain constant. Under these conditions, the magnitude of the DEP force is proportional to the gradient of the square of the electric field strength. Additionally, the direction of the DEP force aligns with the sign of the CM factor. To determine this direction, the CM factor was calculated, as demonstrated in Eq. (3). The average value of the gradient of the square of the electric field strength within the droplet was obtained in our research. This enabled the calculation of the DEP force. Two types of particles, polystyrene microspheres and HEK293 cells, were selected to investigate how changes in the dielectric layer parameters influence the DEP force exerted on these particles. The numerical distribution of CM factors for particles is depicted in Fig. 3(a). According to the graph, the polystyrene microspheres clearly transition from a positive DEP force to a negative DEP force as the frequency increases, whereas the behavior of the HEK293 cells is opposite to that of the polystyrene microspheres. The variations in the DEP force acting on the polystyrene microspheres and HEK293 cells are shown in Figs. 3(b) and 3(c), respectively. At a constant frequency, the DEP force on particles is greater for a dielectric layer of higher permittivity, regardless of the DEP direction. For the negative DEP force on HEK293 cells, the DEP force generated by a dielectric layer with a lower permittivity is insufficient. Therefore, selecting a dielectric layer with a higher permittivity is crucial. According to Fig. 3(d), for the same permittivity of the dielectric layer, an increase in its thickness clearly decreases the DEP force due to a decrease in the gradient of the square of the electric field strength inside the droplet. Additionally, the simulation of the electric field norm of the patterned electrode is shown in Fig. 3(e). The electric field norm is significantly reduced in the areas where electrodes are patterned. As shown in Fig. 3(f), the particles experience a negative DEP force and aggregate in the area with a lower electric field norm. Based on the aforementioned analysis, a higher dielectric layer permittivity and a thinner layer are more favorable for particles to undergo DEP.

From a comprehensive analysis of the droplet and particle manipulation, selecting dielectric layer materials with a high permittivity is found to be favorable for inducing both droplet and particle manipulation. Regarding the thickness, an optimal value that maximizes the EWOD force exists; conversely, a thinner dielectric layer is more beneficial for DEP. Notably, droplet manipulation is more straightforward to achieve than particle manipulation. Therefore, to achieve a larger DEP force, the optimal thickness for droplet manipulation must first be calculated, and then, this parameter must be refined when selecting the dielectric layer. To verify the accuracy of our simulation results, we selected SU-8 and Al_2O_3 as dielectric materials for fabricating DMCs. We then used these chips to conduct droplet and particle driving experiments, as shown in Figs. 4(a) and 4(b) (Multimedia view). During the experiments, we recorded the velocities of the droplets and particles using a camera. We then calculated their acceleration accordingly. As shown in Fig. 4(c), the experimental results demonstrate that the droplet and particle accelerations are consistent with the changing trends of the EWOD force and DEP force. This consistency verifies the effectiveness of our proposed numerical analysis method.

In conclusion, we investigated the effect of dielectric layer parameters on the droplet and particle manipulation within a DMC and conducted experimental validations. Our findings demonstrate that a higher dielectric layer permittivity facilitates enhanced droplet and particle manipulation. Additionally, our studies confirm that there is an optimal dielectric layer thickness for droplet manipulation, while a thinner dielectric layer promotes better particle manipulation. These findings have important guiding significance for selecting the appropriate dielectric layer parameters in the DMC design.

13 November 2024 03:12:15

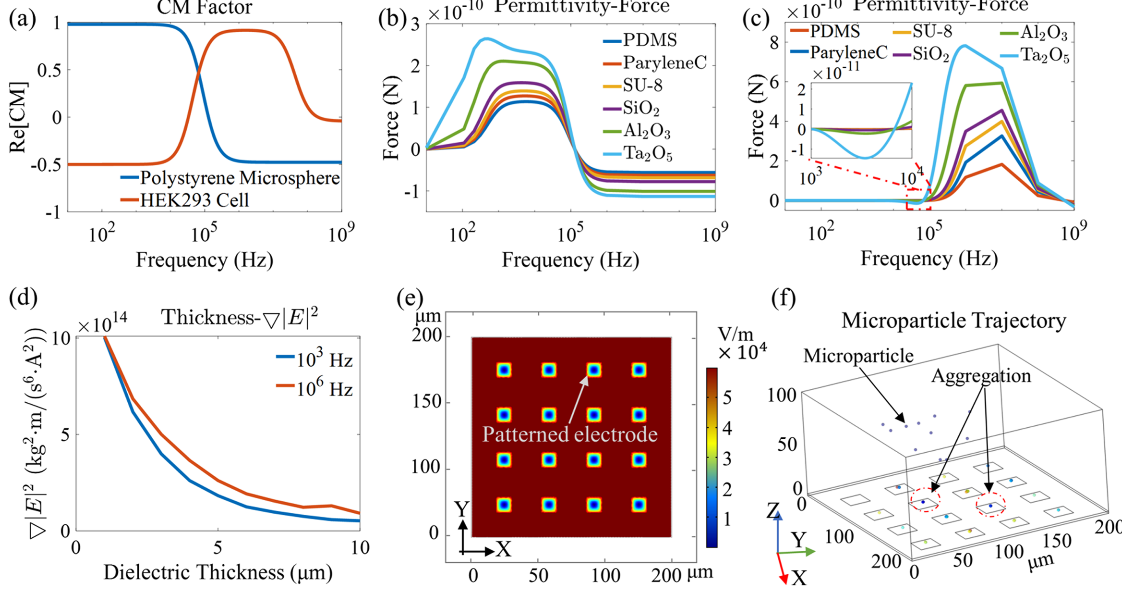

FIG. 3. DEP simulation results. (a) CM factor of the two types of particles. (b) DEP force on polystyrene microspheres at an applied voltage of 10 V. (c) DEP force on HEK293 cells at an applied voltage of 10 V. (d) Correlation between $\nabla|E|^2$ and the dielectric layer thickness (applied voltage = 10 V). (e) Distribution of the electric field norm of the patterned electrode (applied voltage = 10 V). (f) DEP simulation with polystyrene microspheres at an applied voltage = 10 V and time = 30 s.

Published under an exclusive license by AIP Publishing

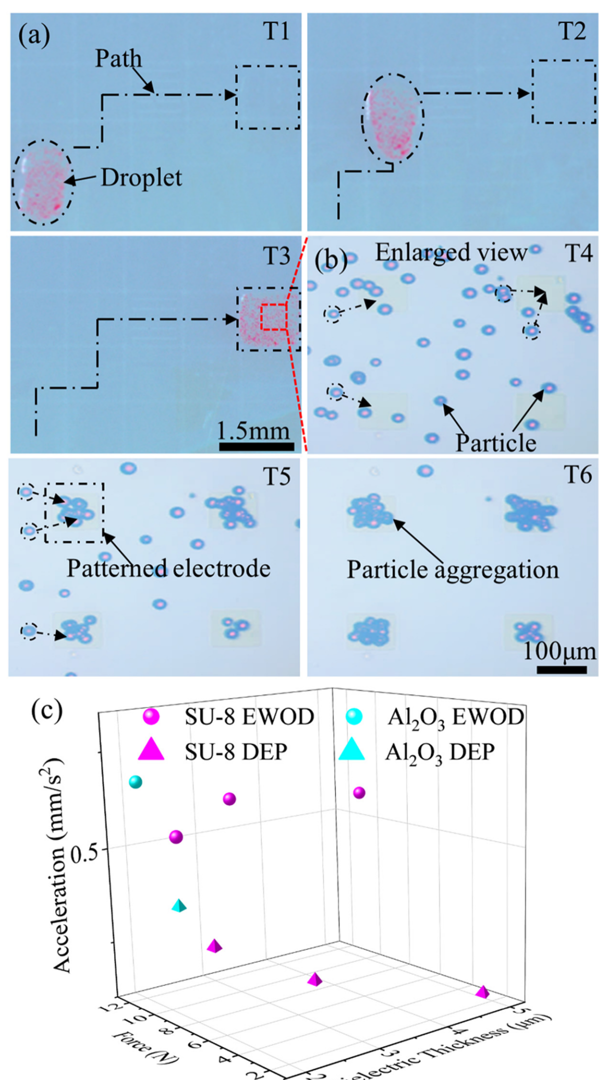

FIG. 4. Experimental results. (a) The droplet is driven along the dotted line based on EWOD. (b) The particles are driven to the patterned electrode based on DEP. (c) Experimental and simulation data verification. (To better illustrate the experimental and simulation data, the EWOD force is multiplied by 10^6, the DEP force is multiplied by 10^{11}, and the particle acceleration is multiplied by 10^2.) Multimedia available online.

See the supplementary material for detailed simulation parameter, the correlation between the EWOD force and the dielectric layer permittivity, and the supporting experimental video.

This research was supported by the National Key Research and Development Program of China (Grant No. 2023YFB4705400), the Beijing Natural Science Foundation (Grant No. 4232055), and the National Natural Science Foundation of China (Grant Nos. 62073042, 62222305, and U22A2064).

AUTHOR DECLARATIONS

Conflict of Interest

The authors have no conflicts to disclose.

Author Contributions

Yanfeng Zhao: Formal analysis (lead); Validation (lead); Writing – original draft (lead); Writing – review & editing (equal). **Menghua Liu:** Investigation (equal); Methodology (equal); Validation (equal). **Xinyi Dong:** Investigation (equal); Methodology (equal); Validation (equal). **Jiaxin Liu:** Investigation (equal); Methodology (equal); Validation (equal); Writing – review & editing (equal). **Hen-Wei Huang:** Investigation (equal); Methodology (equal); Supervision (equal); Validation (equal); Writing – review & editing (equal). **Qing Shi:** Conceptualization (equal); Funding acquisition (lead); Investigation (equal); Supervision (equal); Validation (equal); Writing – review & editing (equal). **Qiang Huang:** Conceptualization (equal); Formal analysis (lead); Funding acquisition (lead); Investigation (equal); Supervision (equal); Writing – original draft (lead); Writing – review & editing (lead). **Huaping Wang:** Conceptualization (equal); Formal analysis (lead); Funding acquisition (lead); Supervision (equal); Validation (equal); Writing – original draft (lead); Writing – review & editing (lead).

DATA AVAILABILITY

The data that support the findings of this study are available from the corresponding author upon reasonable request.

REFERENCES

[1]X. Li, H. Zhu, B. Gu, C. Yao, Y. Gu, W. Xu, J. Zhang, J. He, X. Liu, and D. Li, Adv. Mater. **36**(18), 2305268 (2024).
[2]T. Komatsu, M. Tokeshi, and S. K. Fan, Biosens. Bioelectron. **195**, 113631 (2022).
[3]Q. Ruan, W. Ruan, X. Lin, Y. Wang, F. Zou, L. Zhou, Z. Zhu, and C. Yang, Sci. Adv. **6**(50), eabd6454 (2020).
[4]R. P. S. De Campos, D. G. Rackus, R. Shih, C. Zhao, X. Liu, and A. R. Wheeler, Anal. Chem. **91**(3), 2506–2515 (2019).
[5]Q. Zhang, X. Xu, L. Lin, J. Yang, X. Na, X. Chen, L. Wu, J. Song, and C. Yang, Lab Chip **22**(10), 1971–1979 (2022).
[6]J. Zhai, C. Li, H. Li, S. Yi, N. Yang, K. Miao, C. Deng, Y. Jia, P. I. Mak, and R. P. Martins, Lab Chip **21**(24), 4749–4759 (2021).
[7]L. Cai, L. Lin, S. Lin, X. Wang, Y. Chen, H. Zhu, Z. Zhu, L. Yang, X. Xu, and C. Yang, Small Methods e2400375 (2024).
[8]S. Shen, H. Feng, Y. Deng, S. Xie, Z. Yi, M. Jin, G. Zhou, P. Mulvaney, and L. Shui, Light Sci. Appl. **12**(1), 290 (2023).
[9]M. Y. Chiang, Y. W. Hsu, H. Y. Hsieh, S. Y. Chen, and S. K. Fan, Sci. Adv. **2**(10), e1600964 (2016).
[10]Y. Zhong, H. Yu, P. Zhou, Y. Wen, W. Zhao, W. Zou, H. Luo, Y. Wang, and L. Liu, ACS Appl. Mater. Interfaces **13**(33), 39550–39560 (2021).
[11]C. Hu, H. Zhang, C. Jiang, and H. Ma, Appl. Phys. Lett. **120**(12), 121602 (2022).
[12]C. Hu, K. Jin, and H. Ma, Appl. Phys. Lett. **122**(18), 181601 (2023).
[13]J. Zhai, H. Li, A. H. Wong, C. Dong, S. Yi, Y. Jia, P. I. Mak, C. X. Deng, and R. P. Martins, Microsyst. Nanoeng. **6**, 6 (2020).
[14]M. Khanna, S. Roy, A. Mathur, A. K. Dubey, and R. Vashisth, Mater. Today: Proc. **38**, 179–185 (2021).
[15]S. Türk, A. Schug, R. Viga, A. Jupe, and H. Vogt, Integration **67**, 50–59 (2019).
[16]W. Wang, J. Chen, and J. Zhou, Appl. Phys. Lett. **108**(24), 243701 (2016).
[17]S. K. Fan, Y. W. Hsu, and C. H. Chen, Lab Chip **11**(15), 2500–2508 (2011).
[18]N. Liu, Y. Lin, Y. Peng, L. Xin, T. Yue, Y. Liu, C. Ru, S. Xie, L. Dong, H. Pu, H. Chen, W. J. Li, and Y. Sun, IEEE Trans. Automat. Sci. Eng. **17**(2), 1084–1092 (2020).

13 November 2024 03:12:15

Published under an exclusive license by AIP Publishing